

Supplementary Tables and Figures

Supplementary Table 1: Sample size and minor allele frequency cut-off used in recent eQTL studies

| Study | Tissue/cell type | Sample size | Minor allele frequency cutoff |
|---------------------------|---|-------------|---|
| Brynedal et al., 2017 | lymphocyte cell lines | 83~185 | 15% |
| GTE consortium, 2017 | various tissues (44) | 70~361 | 1% and minor allele count ≥ 10 |
| Kim-Hellmuth et al., 2017 | monocytes (resting and stimulated) | 134 | 5% |
| Ko et al., 2017 | kidney | 96 | 5% |
| Manry et al., 2017 | whole blood (resting and stimulated) | 51 | 10% |
| Ng et al., 2017 | brain | 494 | 1% |
| Pala et al., 2017 | white blood cells | 624 | 1% |
| Peng et al., 2017 | placentas | 159 | minor allele count ≥ 5 (~MAF 1.6%) |
| Yao et al., 2017 | whole blood | 5257 | 1% |
| Chen et al., 2016 | three immune cell types | 197 | minor allele count >4 (~MAF 1.2%) |
| Franzen et al., 2016 | blood and six vascular and metabolic tissues | 600 | 5% |
| Nedelec et al., 2016 | macrophages (resting and stimulated) | 172 | 5% |
| Quach et al., 2016 | monocytes (resting and stimulated) | 200 | 5% |
| Sajuthi et al., 2016 | subcutaneous adipose and skeletal muscle | 256 and 255 | 1% |
| Zhernakova et al., 2016 | whole blood | 2116 | 5% |
| Caliskan et al., 2015 | peripheral blood mononuclear cells (resting and stimulated) | 98 | 10% |
| Hulur et al., 2015 | distal colonic samples | 40 | 5% |
| Kirsten et al., 2015 | peripheral blood mononuclear cells | 2112 | 1% |
| Lock et al., 2015 | blood and brain | 43 | 5% |
| Naranbhai et al., 2015 | peripheral blood CD16+ neutrophils | 101 | 5% |
| Battle et al., 2014 | whole blood | 922 | 2.50% |
| Fairfax et al., 2014 | monocytes (resting and stimulated) | 432 | 4% |
| Hu et al., 2014 | T cells (resting and stimulated) | 174 | 1% |
| Kim et al., 2014 | monocytes (resting and stimulated) | 137 | 5% |
| Kim et al., 2014 | brain | 424 | 1% |
| Lee et al., 2014 | dendritic cells (resting and stimulated) | 534 | 5% |
| Ongen et al., 2014 | tumour and normal colon mucosa samples | 90 | 5% |
| Ramasamy et al., 2014 | 10 brain regions | 134 | 5% |
| Wright et al., 2014 | whole blood | 2494 | 1% |
| Ye et al., 2014 | CD4+ T cells (resting and stimulated) | 348 | 5% |
| Garnier et al., 2013 | monocytes | 758 | 1% |
| Lappalainen et al., 2013 | lymphocyte cell lines | 462 | 5% |
| Li et al., 2013 | tumour samples and normal blood samples | 407 | 5% |
| Westra et al., 2013 | non-transformed peripheral blood | 5311 | 5% |
| Barreiro et al., 2012 | dendritic cells (resting and stimulated) | 65 | 10% |
| Fairfax et al., 2012 | primary monotypes and primary B cells | 283 | 1% |

| | | | |
|------------------------|--|-------------------|----|
| Fu et al., 2012 | blood and four non-blood tissues | 1240 and 62~77 | 5% |
| Grundberg et al., 2012 | adipose, lymphocyte cell lines, and skin | 667~777 | 5% |
| Hao et al., 2012 | lung | 1111 | 1% |
| Stranger et al., 2012 | lymphocyte cell lines | 726 | 5% |

- Brynedal, B. *et al.* Large-Scale trans-eQTLs Affect Hundreds of Transcripts and Mediate Patterns of Transcriptional Co-regulation. *Am J Hum Genet* **100**, 581–591 (2017).
- GTEx Consortium. Genetic effects on gene expression across human tissues. *Nature* **550**, 204–213 (2017).
- Kim-Hellmuth, S. & Lappalainen, T. Concerted Genetic Function in Blood Traits. *Cell* **167**, 1167–1169 (2016).
- Ko, Y.-A. *et al.* Genetic-Variation-Driven Gene-Expression Changes Highlight Genes with Important Functions for Kidney Disease. *Am J Hum Genet* **100**, 940–953 (2017).
- Manry, J. *et al.* Deciphering the genetic control of gene expression following *Mycobacterium leprae* antigen stimulation. *PLoS Genet* **13**, e1006952 (2017).
- Ng, B. *et al.* An xQTL map integrates the genetic architecture of the human brain's transcriptome and epigenome. *Nat Neurosci* **20**, 1418–1426 (2017).
- Pala, M. *et al.* Population- and individual-specific regulatory variation in Sardinia. *Nat Genet* **49**, 700–707 (2017).
- Peng, S. *et al.* Expression quantitative trait loci (eQTLs) in human placentas suggest developmental origins of complex diseases. *Hum Mol Genet* **26**, 3432–3441 (2017).
- Yao, C. *et al.* Dynamic Role of trans Regulation of Gene Expression in Relation to Complex Traits. *Am J Hum Genet* **100**, 571–580 (2017).
- Chen, L. *et al.* Genetic Drivers of Epigenetic and Transcriptional Variation in Human Immune Cells. *Cell* **167**, 1398–1414.e24 (2016).
- Franzen, O. *et al.* Cardiometabolic risk loci share downstream cis- and trans-gene regulation across tissues and diseases. *Science* **353**, 827–830 (2016).
- Nedelec, Y. *et al.* Genetic Ancestry and Natural Selection Drive Population Differences in Immune Responses to Pathogens. *Cell* **167**, 657–669.e21 (2016).
- Quach, H. *et al.* Genetic Adaptation and Neandertal Admixture Shaped the Immune System of Human Populations. *Cell* **167**, 643–656.e17 (2016).
- Sajuthi, S. P. *et al.* Mapping adipose and muscle tissue expression quantitative trait loci in African Americans to identify genes for type 2 diabetes and obesity. *Hum Genet* **135**, 869–880 (2016).
- Zhernakova, D. V. *et al.* Identification of context-dependent expression quantitative trait loci in whole blood. *Nat Genet* **49**, 139–145 (2017).
- Caliskan, M., Baker, S. W., Gilad, Y. & Ober, C. Host genetic variation influences gene expression response to rhinovirus infection. *PLoS Genet* **11**, e1005111 (2015).
- Hulur, I. *et al.* Enrichment of inflammatory bowel disease and colorectal cancer risk variants in colon expression quantitative trait loci. *BMC Genomics* **16**, 138 (2015).
- Kirsten, H. *et al.* Dissecting the genetics of the human transcriptome identifies novel trait-related trans-eQTLs and corroborates the regulatory relevance of non-protein coding locidagger. *Hum Mol Genet* **24**, 4746–4763 (2015).
- Lock, E. F. *et al.* Joint eQTL assessment of whole blood and dura mater tissue from individuals with Chiari type I malformation. *BMC Genomics* **16**, 11 (2015).
- Naranbhai, V. *et al.* Genomic modulators of gene expression in human neutrophils. *Nat Commun* **6**, 7545 (2015).
- Battle, A. *et al.* Characterizing the genetic basis of transcriptome diversity through RNA-sequencing of 922 individuals. *Genome Res* **24**, 14–24 (2014).
- Fairfax, B. P. *et al.* Innate immune activity conditions the effect of regulatory variants upon monocyte gene expression. *Science* **343**, 1246949 (2014).
- Hu, X. *et al.* Regulation of gene expression in autoimmune disease loci and the genetic basis of proliferation in CD4+ effector memory T cells. *PLoS Genet* **10**, e1004404 (2014).
- Kim, S. *et al.* Characterizing the genetic basis of innate immune response in TLR4-activated human monocytes. *Nat Commun* **5**, 5236 (2014).
- Kim, Y. *et al.* A meta-analysis of gene expression quantitative trait loci in brain. *Transl Psychiatry* **4**, e459 (2014).
- Lee, M. N. *et al.* Common genetic variants modulate pathogen-sensing responses in human dendritic cells. *Science* **343**, 1246980 (2014).
- Ongen, H. *et al.* Putative cis-regulatory drivers in colorectal cancer. *Nature* **512**, 87–90 (2014).
- Ramasamy, A. *et al.* Genetic variability in the regulation of gene expression in ten regions of the human brain. *Nat Neurosci* **17**, 1418–1428 (2014).

29. Wright, F. A. *et al.* Heritability and genomics of gene expression in peripheral blood. *Nat Genet* **46**, 430–437 (2014).
30. Ye, C. J. *et al.* Intersection of population variation and autoimmunity genetics in human T cell activation. *Science* **345**, 1254665 (2014).
31. Garnier, S. *et al.* Genome-wide haplotype analysis of cis expression quantitative trait loci in monocytes. *PLoS Genet* **9**, e1003240 (2013).
32. Lappalainen, T. *et al.* Transcriptome and genome sequencing uncovers functional variation in humans. *Nature* **501**, 506–511 (2013).
33. Li, Q. *et al.* Integrative eQTL-based analyses reveal the biology of breast cancer risk loci. *Cell* **152**, 633–641 (2013).
34. Westra, H.-J. *et al.* Systematic identification of trans eQTLs as putative drivers of known disease associations. *Nat Genet* **45**, 1238–1243 (2013).
35. Barreiro, L. B. *et al.* Deciphering the genetic architecture of variation in the immune response to *Mycobacterium tuberculosis* infection. *Proc Natl Acad Sci U S A* **109**, 1204–1209 (2012).
36. Fairfax, B. P. *et al.* Genetics of gene expression in primary immune cells identifies cell type-specific master regulators and roles of HLA alleles. *Nat Genet* **44**, 502–510 (2012).
37. Fu, J. *et al.* Unraveling the regulatory mechanisms underlying tissue-dependent genetic variation of gene expression. *PLoS Genet* **8**, e1002431 (2012).
38. Grundberg, E. *et al.* Mapping cis- and trans-regulatory effects across multiple tissues in twins. *Nat Genet* **44**, 1084–1089 (2012).
39. Hao, K. *et al.* Lung eQTLs to help reveal the molecular underpinnings of asthma. *PLoS Genet* **8**, e1003029 (2012).
40. Stranger, B. E. *et al.* Patterns of cis regulatory variation in diverse human populations. *PLoS Genet* **8**, e1002639 (2012).

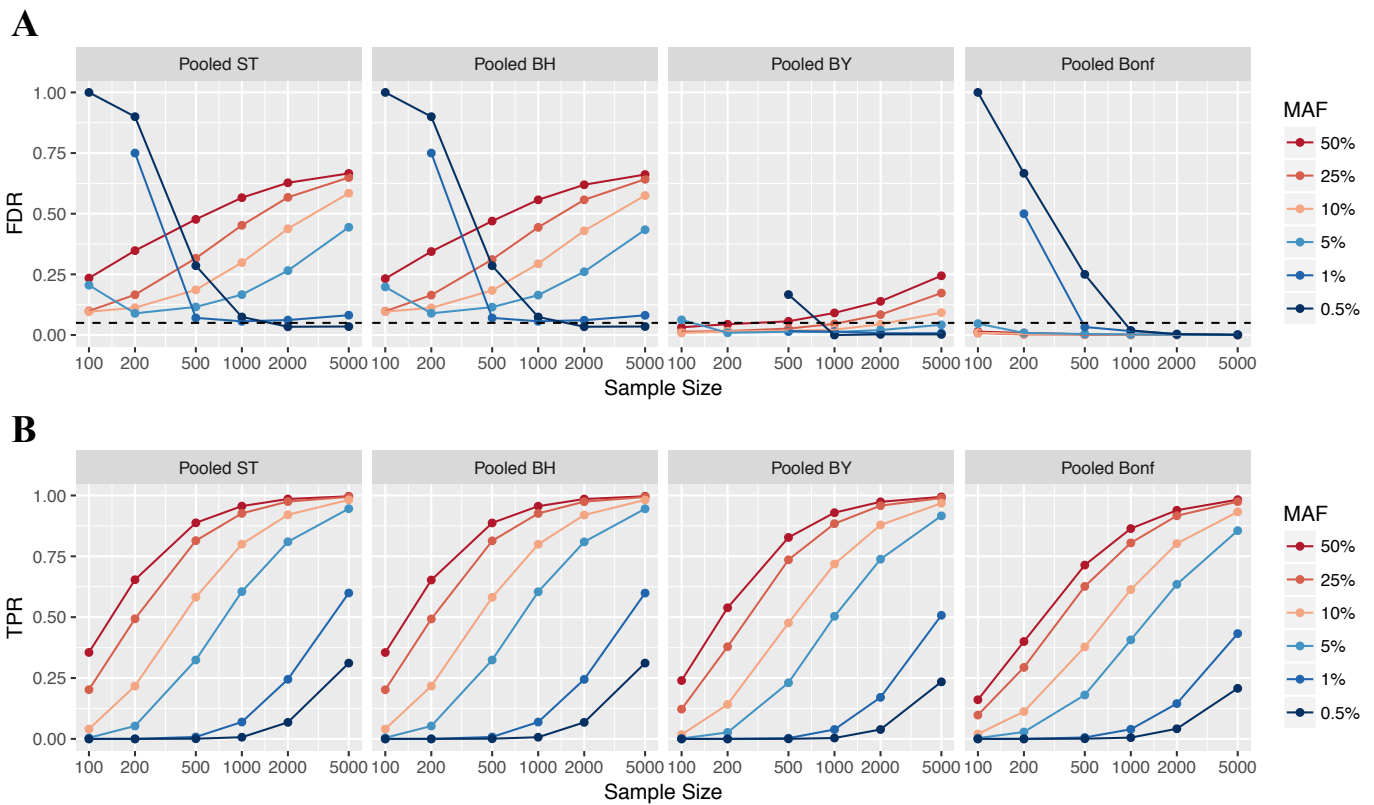


Figure S1. False discovery rate (FDR) and sensitivity of pooled methods for increasing sample sizes. Each panel represents a pooled multiple testing correction method, namely Storey-Tibshirani (ST), Benjamini-Hochberg (BH), Benjamini-Yekutieli (BY), and Bonferroni. FDR (**A**) and sensitivity/true positive rate (TPR) (**B**) calculated from 100 simulations are shown on y-axes and sample sizes are shown on x-axes. Each dot represents one simulation scenario and are coloured according to the simulated causal eSNP minor allele frequency (MAF). The dashed horizontal line indicates the desired FDR level of 5%. Missing dots for sample sizes in panel **A** are scenarios in which no significant eGenes were identified (the corresponding sensitivity in panel **B** is 0).

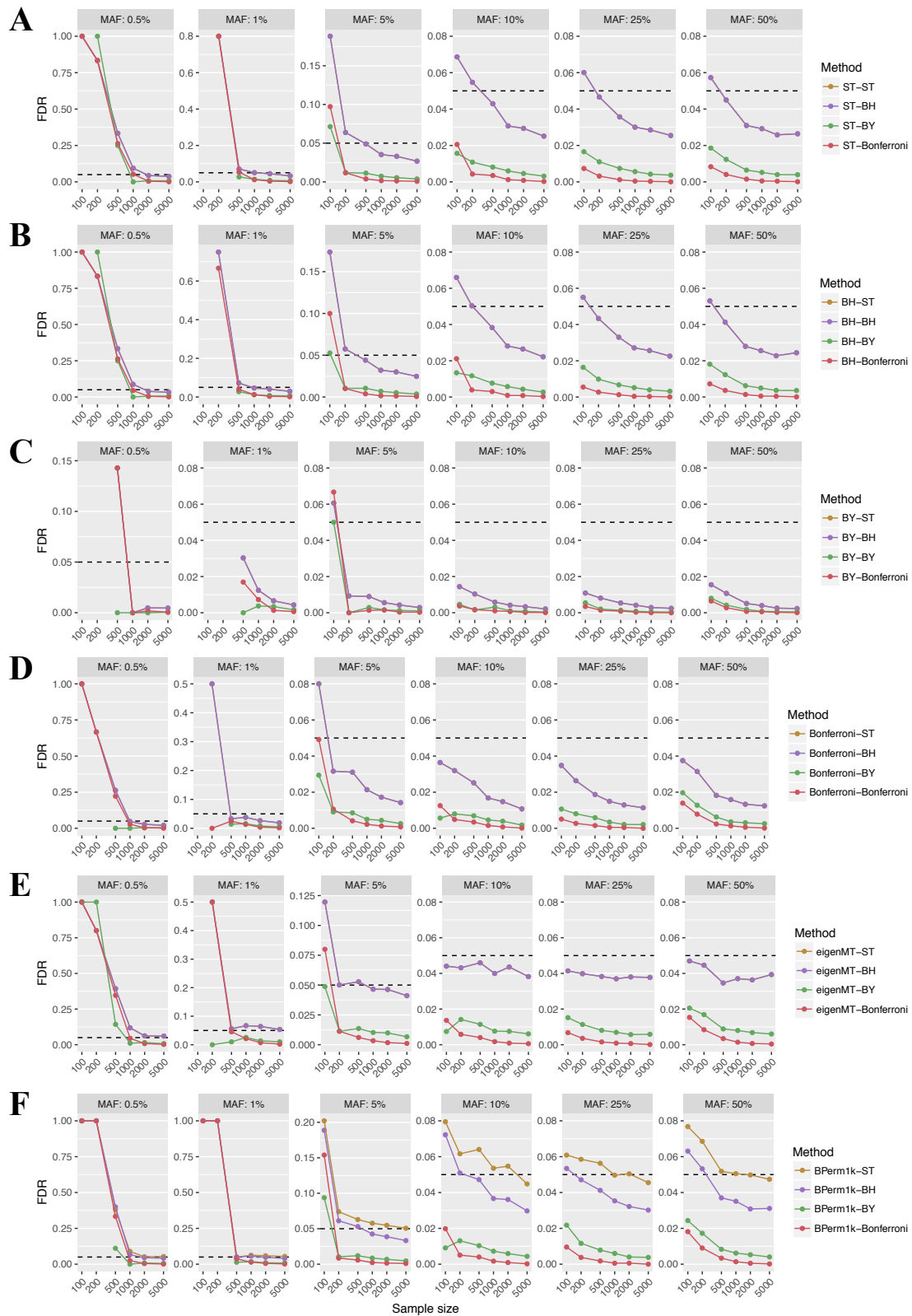


Figure S2. False discovery rate (FDR) of all hierarchical multiple testing correction methods. In each of row, we compared four methods applied in the global correction step of hierarchical correction procedures, which aims to correct for multiple genes being tested: the Storey-Tibshirani (ST), Benjamini-Hochberg (BH), Benjamini-Yekutieli (BY) FDR procedures, and the Bonferroni correction. Rows represent different methods (ST, BH, BY, Bonferroni, eigenMT, and permutation approach) used in the local correction step of hierarchical correction procedures, which aims to correct for multiple SNPs tested for each gene. Scenarios where true eSNPs had different minor allele frequencies (MAFs) are shown in different plots and sample size is shown on x-axes. The dashed horizontal line indicates the desired FDR level of 5%. Use of BY and Bonferroni for global correction had lower FDR than ST and BH. Note that the use of ST and BH for global correction had the same FDR except when permutation approaches were used for local correction.

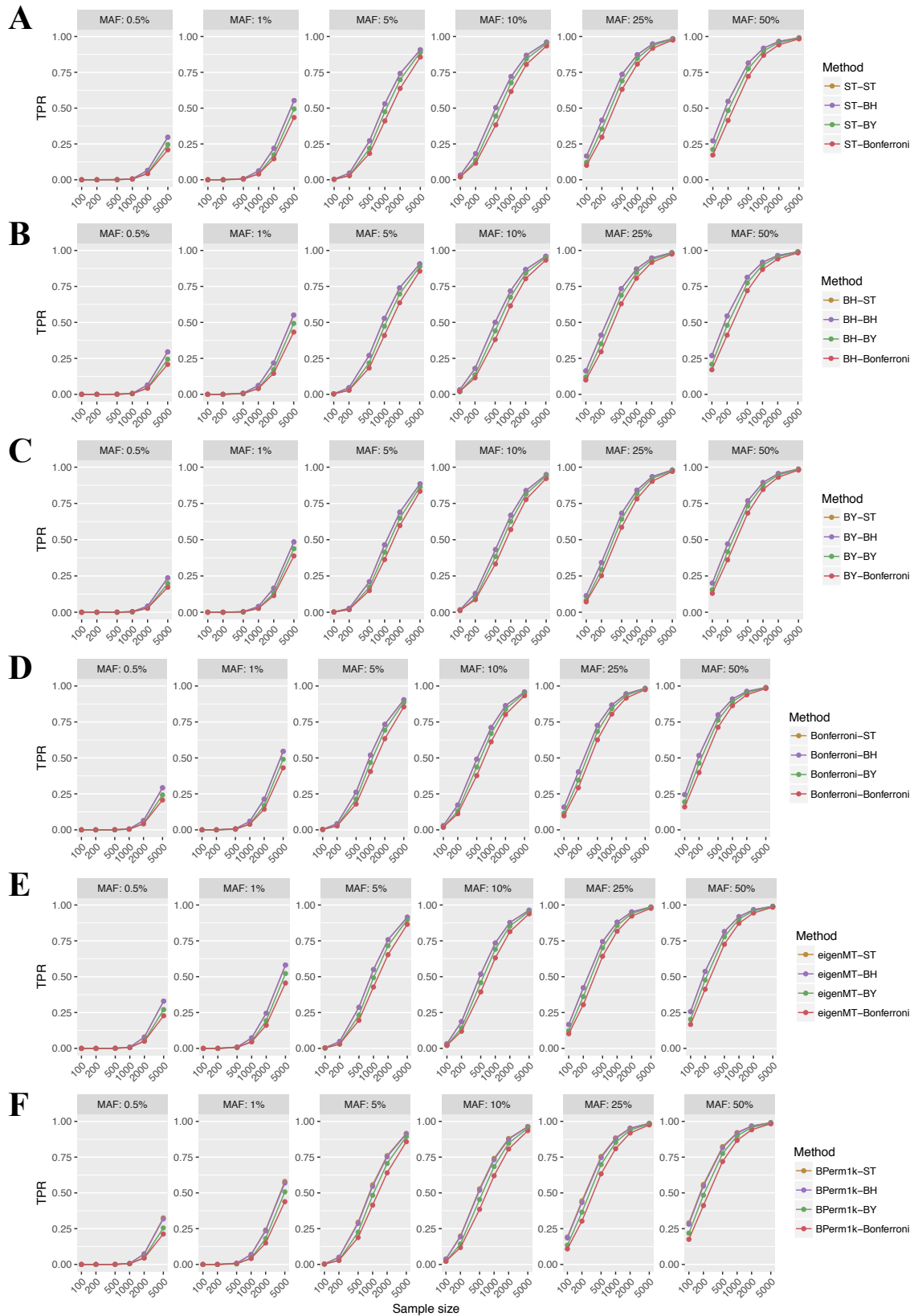


Figure S3. Sensitivity/true positive rate (TPR) of all hierarchical multiple testing correction methods. In each row, we compared four methods applied in the global correction step of hierarchical correction procedures, which aims to correct for multiple genes being tested: the Storey-Tibshirani (ST), Benjamini-Hochberg (BH), Benjamini-Yekutieli (BY) FDR procedures, and the Bonferroni correction. Rows represent different methods (ST, BH, BY, Bonferroni, eigenMT, and permutation approach) used in the local correction step of hierarchical correction procedures, which aims to correct for multiple SNPs tested for each gene. Scenarios where true eSNPs had different minor allele frequencies (MAFs) are shown in different plots and sample size is shown on x-axes. Use of BY and Bonferroni for global correction had lower sensitivity than ST and BH. Note that use of ST and BH for global correction had the same sensitivity except when permutation approaches were used for local correction.

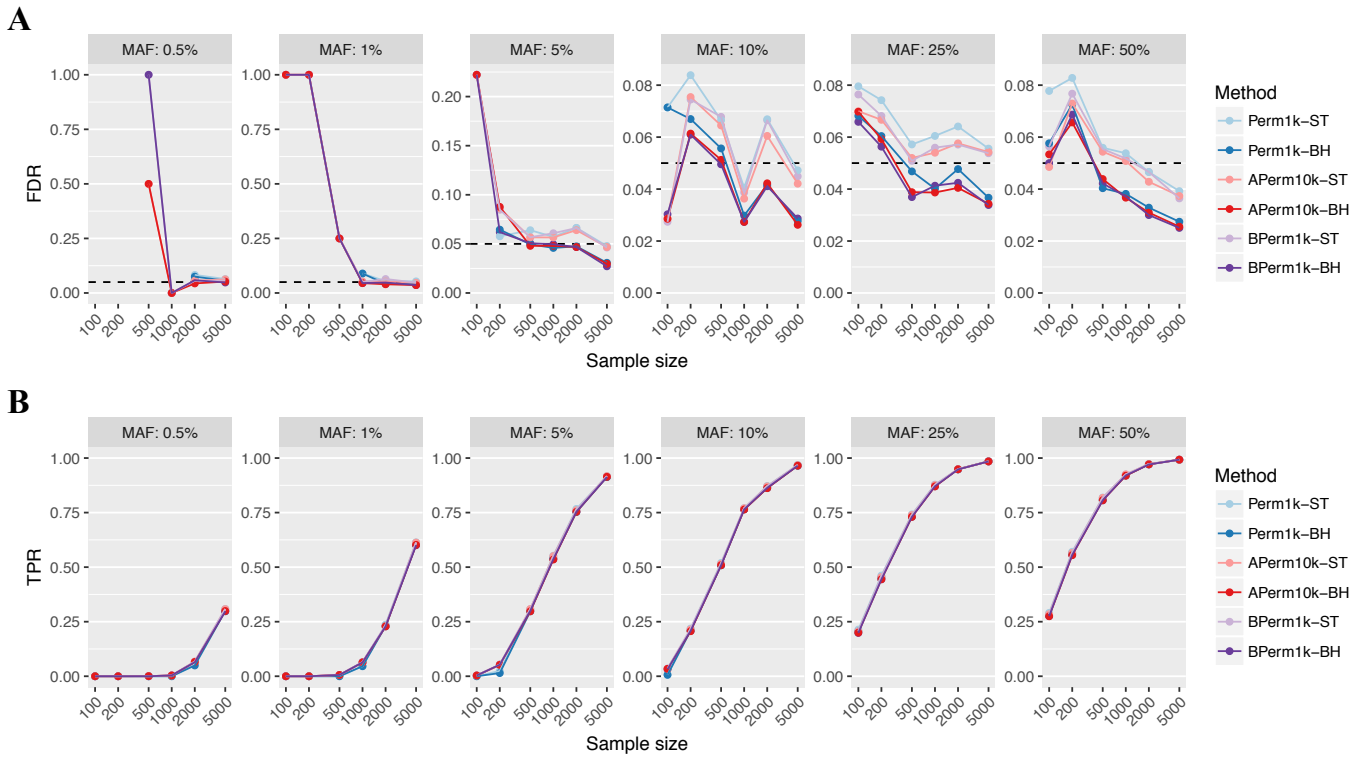


Figure S4. False discovery rate (FDR) and sensitivity of hierarchical multiple testing correction using permutation tests. FDR (A) and sensitivity/true positive rate (TPR) (B) of three permutation approaches (different colours) used in the local correction step of hierarchical correction procedures from 10 simulations are shown on y-axes: using exact permutation p-values obtained from 1,000 permutations (Perm1k), p-values obtained from beta approximation from 1,000 permutations (BPerm1k), and p-values obtained from a beta approximation scheme with a minimum of 100 and maximum of 10,000 permutations (APerm10k). Benjamini-Hochberg (BH) or Storey-Tibshirani (ST) FDR procedure were used in the global correction step of hierarchical correction procedures to correct for multiple genes. Each dot represents one scenario and plots show scenarios with different causal eSNP MAFs. The horizontal line indicates the desired FDR level of 5%. FDR was not calculated for scenarios where no significant eGenes were identified.

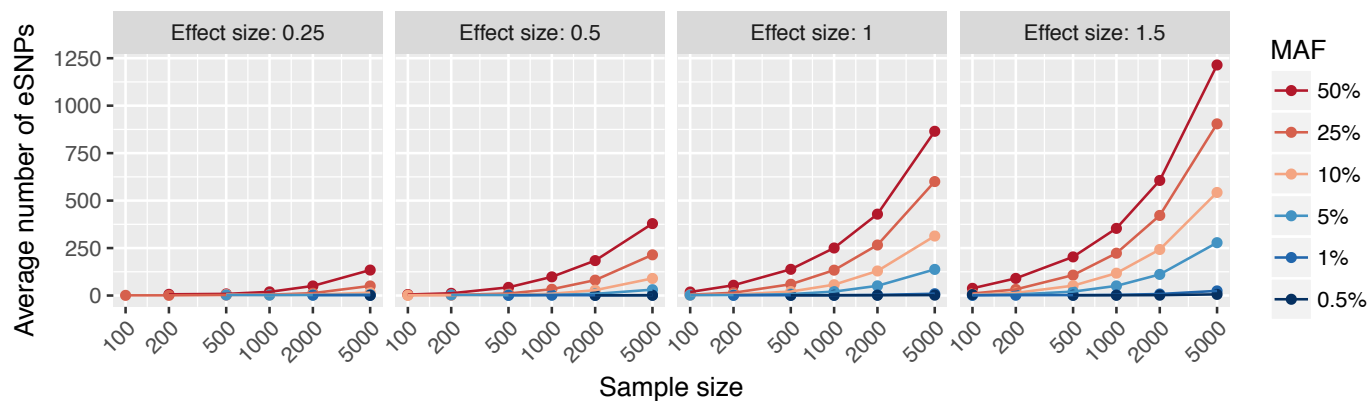


Figure S5. Average number of significant eSNPs per true positive eGene. For each scenario where a constant effect size (0.25, 0.5, 1.0, or, 1.5 s.d. gene expression per allele) was simulated, the average number of eSNPs significantly associated with each true positive eGene was calculated (y-axes). A hierarchical correction procedure using eigenMT for local correction and BH for global correction (eigenMT-BH) was used to correct for multiple testing. Sample size is shown on x-axes and colors of dots indicate varying minor allele frequencies (MAFs) of true eSNPs.

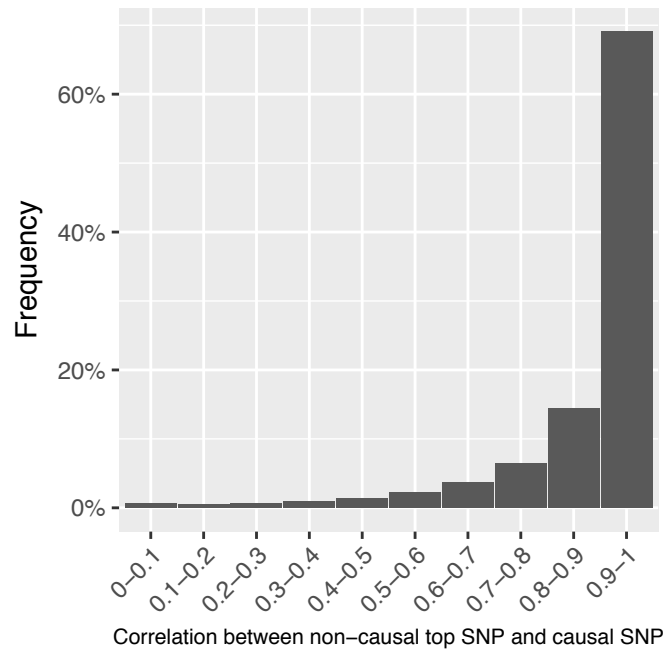


Figure S6. Histogram of linkage disequilibrium (LD) r^2 between the top SNPs that were not causal and their respective causal eSNPs. For every true positive eGene, we calculated the LD r^2 between the top SNP and the simulated causal eSNP. Histogram bins show the percentage of non-causal top SNPs with the given r^2 LD range to the causal eSNP calculated across 100 simulations of all 144 scenarios where a constant effect size was simulated. A hierarchical correction procedure using eigenMT for local correction and BH for global correction (eigenMT-BH) was used to correct for multiple testing. 83% of non-causal top SNPs had an $r^2 \geq 0.8$ with their respective causal eSNP.

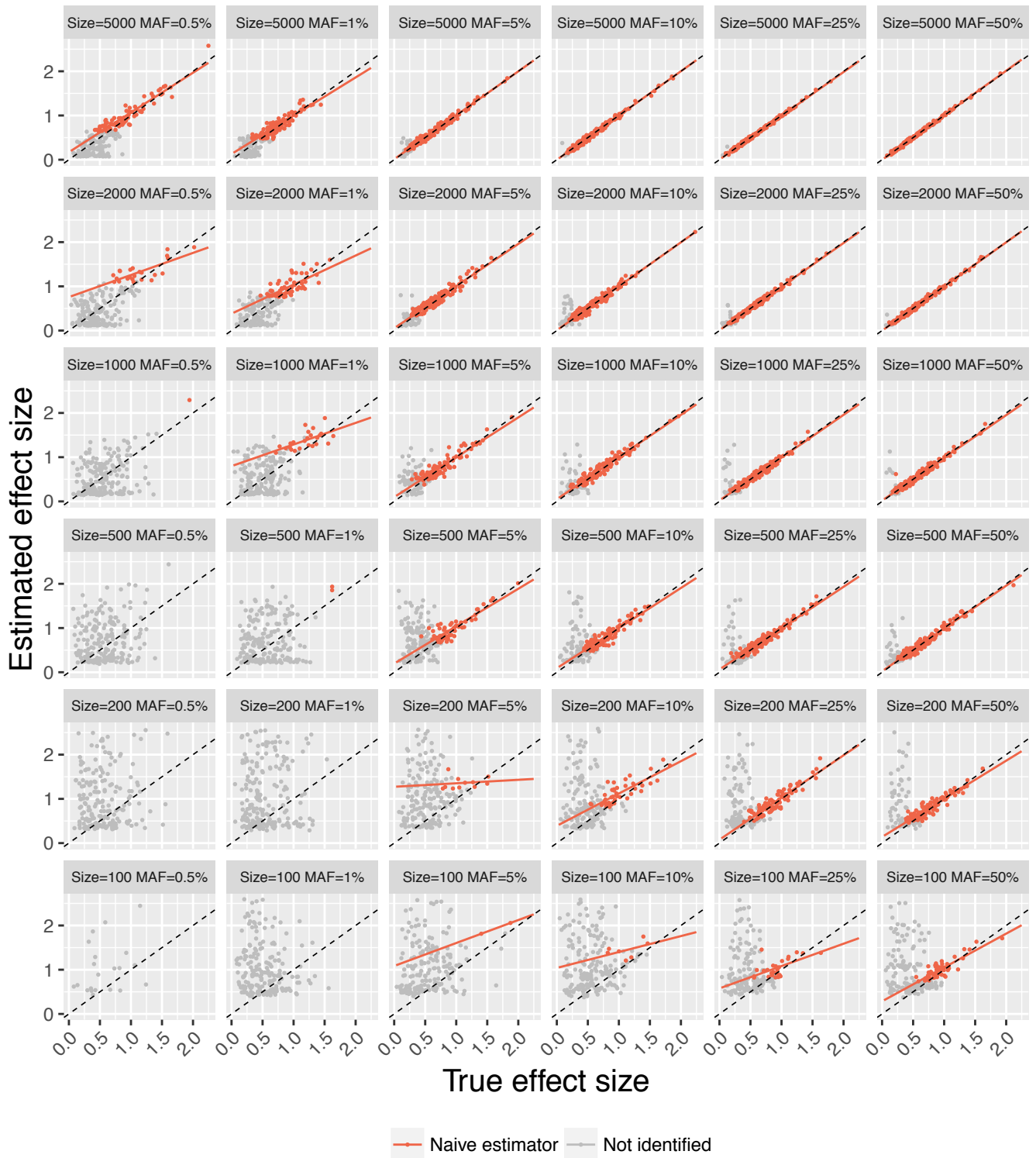


Figure S7. Winner's Curse in eQTL effect size estimation. Each plot represents one scenario, with sample size increasing from bottom to top and minor allele frequency (MAF) of true eSNPs increasing from left to right. Estimated effect sizes are shown on y-axes (naïve estimator from linear regression) and simulated true effect sizes are on x-axes. Each dot represents the top SNP of a true simulated eGene. True positive eGenes are coloured red and grey dots are simulated true eGenes that were not significant after hierarchical multiple testing correction using eigenMT for local correction and BH for global correction (eigenMT-BH). Dashed diagonals indicate where the estimated effect size equals to the true value. Red lines are linear regression fit of the naïve estimator on the simulated effect size for the true positive eGenes.

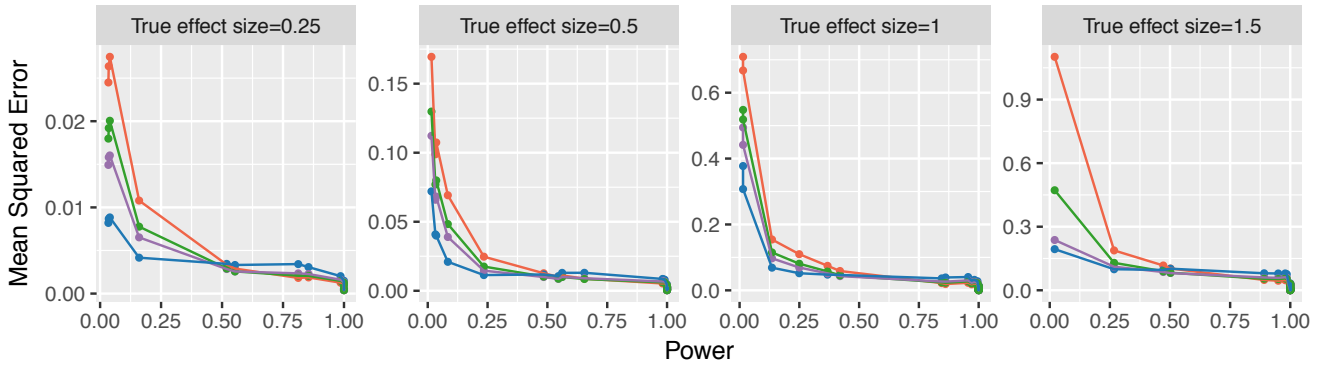
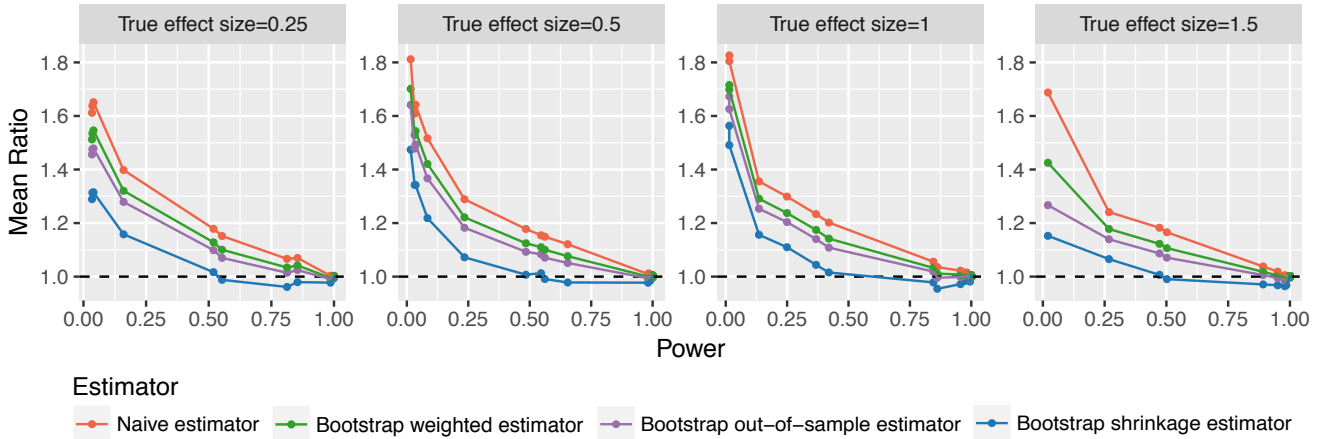
A**B**

Figure S8. Accuracy of three bootstrap estimators and the naïve estimator. Three bootstrap estimators as well as the naïve estimator (different colours) were compared by calculating their mean squared error (MSE) with the simulated true effect size (**A**) and the mean ratio of estimated effect size to the simulated true effect size (**B**) from 10 simulations of scenarios where a constant true effect size (0.25, 0.5, 1, or, 1.5 s.d. gene expression per allele) was simulated in each scenario. A hierarchical correction procedure using eigenMT for local correction and BH for global correction (eigenMT-BH) was used to correct for multiple testing. The horizontal line in panel **B** indicates the ideal unbiased estimator, with mean ratio at one.

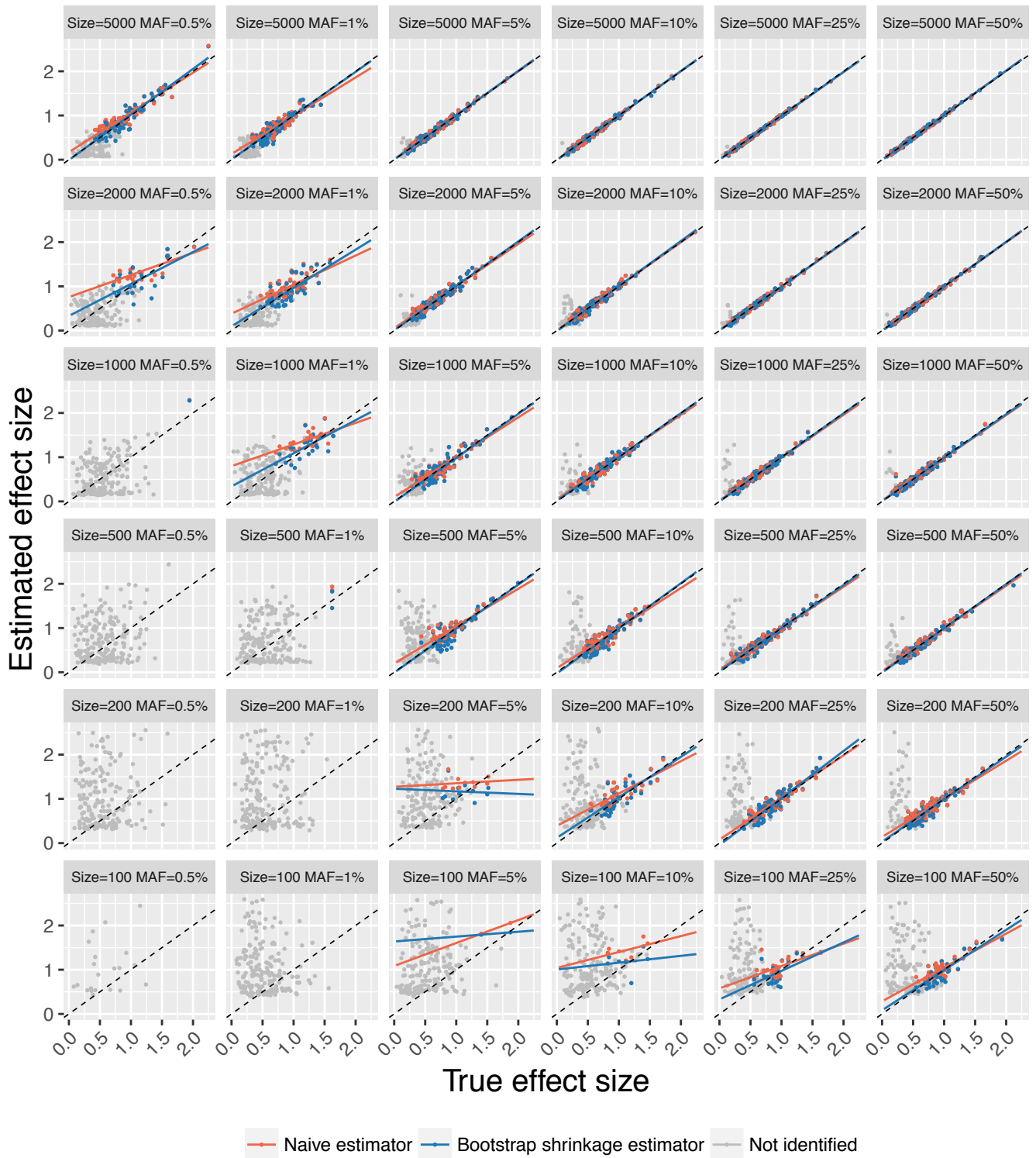


Figure S9. Correction for Winner's Curse by bootstrap method. Each plot represents one scenario, with sample size increasing from bottom to top and minor allele frequency (MAF) of true eSNPs increasing from left to right. Estimated effect sizes are shown on y-axes and true simulated effect sizes are on x-axes. Each dot represents the top SNP of a true simulated eGene. True positive eGenes are coloured red (naïve estimator) or blue (bootstrap shrinkage estimator), and grey dots are true eGenes that were not significant after hierarchical multiple testing correction using eigenMT for local correction and BH for global correction (eigenMT-BH). Dashed diagonals indicate where the estimated effect size equals the true simulated effect size. Red (or blue) lines are linear regression fit of the naïve estimator (or bootstrap shrinkage estimator) on the simulated effect size for the true positive eGenes.